Unidirectional propagation of single photons realized by a scatterer coupled to whispering-gallery-mode microresonators

Cong-Hua Yan [1], Ming Li [2], Xin-Biao Xu,[2] Yan-Lei Zhang [2], Xin-Yue Ma,[1] and Chang-Ling Zou [2,3,*]

[1]*College of Physics and Electronic Engineering, Sichuan Normal University, Chengdu 610068, China*

[2]*CAS Key Laboratory of Quantum Information, University of Science and Technology of China, Hefei, Anhui 230026, China*

[3]*State Key Laboratory of Quantum Optics and Quantum Optics Devices, Shanxi University, Taiyuan 030006, China*

Coherently manipulating single photons in nanophotonic structures with unidirectional propagation is one of the central goals for integrated quantum information processing. Photonic devices constructed by a single atom coupled to a whispering-gallery-mode microresonator (WGMM) with nonideal chiral photon-atom interactions inevitably induce undesired photon scattering. Here, an external scatterer is introduced to the WGMM to cancel the reflection of signal photons by an atom due to nonideal chiral interactions. By properly tuning the positions of the scatterer, destructive and constructive interferences between reflected photons of different pathways are utilized to control the reflection properties of single incident photons. The results show that the reflection probabilities can be suppressed by applying the interplay between chirality and backscattering. Constructing perfect destructive interferences directly leads to unidirectional propagation even when the photon-atom interactions are not ideal. Because the amplitudes of the reflected photons produced by the scatterer can be enhanced to meet requirements of perfect destructive interfering processes, unidirectional propagation is preserved against dissipations.

I. INTRODUCTION

Photons are ideal information carriers due to their ultrafast transmission speed and minimum interactions with the environment and themselves [1–5]. Therefore, manipulating quantum information carried by single photons in photonic circuits has long been the driving force behind the effort to construct a quantum internet [6–8]. In particular, controlling the unidirectional propagation of single photons (UPSP) by switches [9,10], routers [11], and diodes [12] is crucial to realize cascade quantum systems [13]. To ensure proper operations of such quantum optical devices, parasitic reflections between optical devices must be completely suppressed at the single-photon level, as such feedback can have deleterious effects on the operation of optical devices based on interferometric designs [12]. Accordingly, considerable effort has been invested toward the achievement of UPSP by utilizing the essential properties of photons such as frequencies [9], amplitudes [14], and phases [15,16].

In the last decade, another intrinsical property of the photon as circular polarizations provided a prospective capacity to realize UPSP of single photons in photonic waveguides and nanofibers [17]. In these nanophotonic structures, light was strongly confined transversely and generally led to longitudinal components of the electric field. Consequently, the electric field was circularly polarized and therefore carried spin angular momentum [18]. If such spin-momentum-lock light is coupled to quantum emitters with polarization-dependent dipole transitions, then direction-dependent emission, scattering, and absorption of single photons, known as chiral quantum optics, are obtained [17]. For example, when two emitters with right-hand circular polarization σ_+ are coupled to the waveguide with ideal chiral photon-atom interactions, an arbitrary superposition state stored in emitter 1 could be mapped to emitter 2 with unity efficiency by a rightward-propagating photon. Within the framework of chiral quantum optics, it becomes possible to realize cascaded quantum systems [19–26]. However, the chiral photon-atom interaction crucially depends on both the local electric field and the polarization of the atomic transition dipole moment [27–29]. Ideal chirality (i.e., light emitting in just a single direction) is obtained by strictly placing the circular dipole at the point of perfect circular polarization. These points are scarce because only elliptical polarization is practically accessible in nanofiber waveguides [20]. Although an atom placed at the singular point of glide-plane photonic crystal waveguides (i.e., known as the C-point) can display a spin-dependent unidirectional emission, the corresponding photon-atom interaction is relatively small [30]. It indicates that the light field is elliptically polarized over the majority of the mode volume with strong photon-atom interaction [31]. This forces a compromise between strong photon-emitter interactions and makes those interactions with high chiralities. Consequently, photon-atom interactions in real experiments are nonideal chiral [30,32]. Therefore, the incident photon is inevitably reflected with information backflow, which directly suppresses the efficiency of information transfer.

Actually, this chiral photon-atom interaction can also be obtained with an atom coupled to a whispering-gallery-mode

microresonator (WGMM), wherein the two degenerate modes of opposite circling directions in the WGMM with orthogonal circular polarizations are used [33–35]. As a result of their highly confined mode volumes and ultrahigh quality factors, WGMMs enable strong chiral photon-atom interactions that can be utilized to realize UPSP devices at the single photon level, such as a circulator (coupling with a V-type three-level atom [36]) and a router (coupling with a Λ-type three level atom) [37]. The operation condition for these devices is that each atomic transition is exclusively coupled to only one WGMM mode. Meanwhile, the unidirectional coupling of multiple two-level atoms to a chiral ring resonator results in chiral quantum optomechanics and induces quantum phase transition [38]. However, the electric field polarizations at the positions of the atoms depend on both the distance to the resonator surface and the ratio between longitudinal and transversal electric field components [33]. The ratio determined by the refractive index of the resonator material approximate 0.7 leads the electric field of the WGMM to be elliptical [33,39]. Therefore, the atom is simultaneously coupled to the two degenerate WGMM modes and thus both forward and backward emission rates from the atom exist [37,40]. As a result, the incident photons always have backflow in these UPSP devices.

Recently, WGMMs perturbed by nanoparticles such as nanotips have been of particular interest in the context of modern sensing applications [41,42]. It is well known that a single nanoparticle placed in the evanescent field of a WGMM leads to coherent backscattering coupling between clockwise (CW) and counterclockwise (CCW) propagating modes [43]. This mode coupling between the CW and CCW modes lifts the spectral degeneracy and gives rise to splittings with two dips in the transmission spectra of the WGMM [44]. Two scatterers placed within the mode volume of the WGMM are used to tune the coupling between the CW and CCW modes. When the relative positions and effective sizes of the scatterers are finely tuned, only one of the traveling directions is dominant [45–47].

In this work, a scatterer and an atom simultaneously coupled to a WGMM are adopted to manipulate the transporting properties of single photons. Although the coupling between the two-level atom and the WGMM is nonideal chiral, the reflection of the incident single photon can be sufficiently suppressed by controlling the interplay between chirality and backscattering. In particular, when the two conditions for perfect destructive interference between photons from different pathways are satisfied, the UPSP arises. By properly tuning the positions of the scatterer and adjusting the frequency of the photon, the amplitudes of the photon produced by the scatterer can be enhanced to preserve the perfect destructive interference, and consequently, unidirectional propagation is maintained for the dissipative case.

This paper is organized as follows. The model is described in Sec. II by directly calculating the response of such a system to a single injected photon. Section III discusses the interplay between chirality and backscattering. The UPSP against dissipations is investigated in Sec. IV. Finally, we conclude our work and suggest experimental demonstrations of our proposal with current photonic techniques in Sec. V.
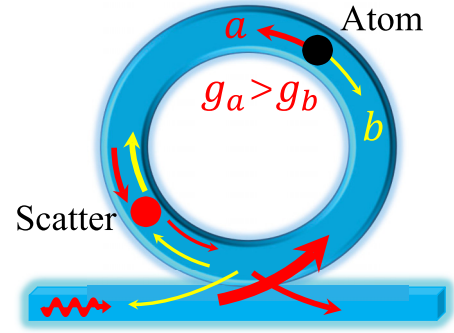

FIG. 1. Schematic diagram of the interplay between chirality and backscattering in a microresonator. A single photon depicted as a wiggly wave is incident from the left side of the waveguide. A scatterer (a red ball) and a two-level atom (a black ball) with a right-hand circularly polarized transition (σ_+ transition) are coupled to a WGMM. The electric field at the position of the atom is elliptically polarized and thus the photon-atom interaction is nonideal chiral. The nonideal chirality leads the atom asymmetrically coupling to both the CW and CCW propagating modes in the WGMM (i.e., simplified as modes b and a) with different coupling strengths as $g_a > g_b$.

II. MODEL AND SOLUTIONS

The schematic of the system to realize the UPSP with nonideal chiral photon-atom interactions between a WGMM and a two-level atom is shown in Fig. 1. Due to the cavity evanescent electric field at the position of the atom being elliptically polarized, the atom coupled to both the CW and CCW modes with different coupling strengths. When the resonance energy of the atom is far from the cutoff frequency of the dispersion relations of the WGMM and the waveguide, the effective Hamiltonian of the system in real space under the rotating wave approximation with modeling the single-excitation is given by (with $\hbar = 1$) [9,48–50]

$$H = H_{\text{cav}} + H_{\text{JC}} + H_{\text{BS}}, \tag{1}$$

wherein

$$
\begin{aligned}
H_{\text{cav}} = {} & \int dx\, C_R^\dagger(x)\left(\omega_0 - iv_g\frac{\partial}{\partial x}\right)C_R(x) \\
& + \int dx\, C_L^\dagger(x)\left(\omega_0 + iv_g\frac{\partial}{\partial x}\right)C_L(x) \\
& + \left(\omega_c - i\frac{1}{\tau_a}\right)a^\dagger a + \left(\omega_c - i\frac{1}{\tau_b}\right)b^\dagger b \\
& + \int dx\,\delta(x)[V_a C_R^\dagger(x)a + V_a^* a^\dagger C_R(x)] \\
& + \int dx\,\delta(x)[V_b C_L^\dagger(x)b + V_b^* b^\dagger C_L(x)],
\end{aligned}
\tag{2}
$$

describes the cavity-waveguide system, the Jaynes-Cumming interaction Hamiltonian

$$
\begin{aligned}
H_{\text{JC}} = {} & \left(\Omega - i\frac{1}{\tau_2}\right)\sigma_{22} + (j_a a\sigma_{21} + j_a^* a^\dagger \sigma_{12}) \\
& + (j_b b\sigma_{21} + j_b^* b^\dagger \sigma_{12}),
\end{aligned}
\tag{3}
$$

describes the atom-cavity-mode interaction, and

$$H_{\text{BS}} = r(e^{i\xi}ba^{\dagger} + e^{-i\xi}b^{\dagger}a) \qquad (4)$$

is the backscattering-induced intermode coupling. Here, $C_R^{\dagger}(z)$ [$C_L^{\dagger}(x)$] is the creation operator for a right-going (left-going) photon of frequency ω at the x position of the waveguide. ω_0 is a reference frequency, around which the waveguide dispersion relation is linearized. $a^{\dagger}$ ($b^{\dagger}$) is the creation operator for the CCW (CW) mode with the same frequency of ω_c and dissipation rates of $1/\tau_a$ ($1/\tau_b$). σ_{ij} is the atomic operator $|i\rangle\langle j|$ with the atom transition frequency Ω and the excited state dissipation rate of $1/\tau_2$. V_a and V_b are the coupling strengths of different modes to the waveguide. Typically, the right-moving (left-moving) photon only couples to the CCW (CW) mode of the WGMM. As we are only interested in a narrow range in the vicinity of the atomic resonant frequency, V_a and V_b are safely assumed to be independent of frequency [10,11,51]. Physically, such an assumption is equivalent to a Markovian approximation [48]. The Dirac delta function $\delta(x)$ indicates that the WGMM is near the location $x = 0$ of the waveguide. $j_a = -\vec{\phi}_a \cdot \vec{d}$ and $j_b = -\vec{\phi}_b \cdot \vec{d}$ are the coupling strengths between the atom and the WGMM modes [49,52–54]. $\vec{\phi}_a$ and $\vec{\phi}_b$ are the electric field profiles of modes a and b. $\vec{d}$ is the atomic dipole vector. When the transition from the excited state to the ground state corresponds to the difference in the magnetic quantum number of $\Delta_{m_F} = +1$, $\vec{d}$ is necessarily a complex vector. Consequently, the coupling strengths of j_a and j_b are complex numbers [49,50] for the atom coupling to the pair of degenerate WGMM modes, which gives $\vec{\phi}_a = \vec{\phi}_b^*$ and thus $|j_a| \neq |j_b|$ [49]. Therefore, we can simplify the coupling strengths as $j_a = g_a e^{i\theta}$ and $j_b = g_b e^{-i\theta}$ with $g_a > g_b$. $re^{i\xi}$ is the intermode coupling strength due to backscattering, with phase ξ depending on the relative position between the scatterer and the atom [55]. Experimentally, the effective size (denoted by r) of the scatterer (i.e., the overlap between the scatterer and the mode volume of the WGMM) can be precisely controlled by a nanopositioner, while the quality factor of the WGMM is nearly unaffected by the scatterer [45–47].

In this work, we concentrate on manipulating the UPSP by utilizing the interplay between chirality and backscattering in the WGMM. The single photon is injected from the left side of the waveguide and the atom is originally prepared in the ground state. After being scattered by the cavity-atom-scatterer system, the incident single photon may be absorbed by the atom, may excite modes of the WGMM, and may also be scattered to the left or right directions along the waveguide. Generally, in the case of single-photon transport, a single-photon pulse has a duration that is much longer than the spontaneous lifetime of the atom [56]. Therefore, the general eigenstate of the system should take the following form:

$$|\psi\rangle = \int dx[\phi_R C_R^{\dagger}(x) + \phi_L C_L^{\dagger}(x)]|0_w, g\rangle$$
$$+ e_a a^{\dagger}|0_w, g\rangle + e_b b^{\dagger}|0_w, g\rangle + e_2 \sigma_{21}|0_w, g\rangle, \quad (5)$$

where $|0_w, g\rangle$ is the vacuum, with zero photon in the waveguide and the atom in the ground state. e_a, e_b, and e_2 are the excitation amplitudes of mode a, mode b, and the atom, respectively. The spatial dependence of wave functions can be expressed as

$$\phi_R = e^{ikx}\theta(-x) + t_u e^{ikx}\theta(x), \qquad (6)$$

$$\phi_L = r_u e^{-ikx}\theta(-x), \qquad (7)$$

where $\theta(x)$ is the step function, and $k = (\omega - \omega_0)/v_g$. $T = |t_u|^2$ and $R = |r_u|^2$ give the transmission and reflection probabilities of an input photon with frequency ω, respectively. Following the procedure in Refs. [9,16,48,49,57,58] that directly dealt with the photon scattering eigenstates in real space, the time-independent Schrödinger equation $H|\psi\rangle = \omega|\psi\rangle$ yields

$$-iv_g\frac{\partial}{\partial x}\phi_R(x) + \delta(x)V_a e_a = (\omega - \omega_0)\phi_R(x), \qquad (8)$$

$$iv_g\frac{\partial}{\partial x}\phi_L(x) + \delta(x)V_b e_b = (\omega - \omega_0)\phi_L(x), \qquad (9)$$

$$\left(\omega_a - i\frac{1}{\tau_c}\right)e_a + V_a^*\phi_R(0) + g_a e^{-i\theta}e_q + re^{-i\xi}e_b = \omega e_a, \qquad (10)$$

$$\left(\omega_b - i\frac{1}{\tau_c}\right)e_b + V_b^*\phi_L(0) + g_b e^{i\theta}e_q + re^{i\xi}e_a = \omega e_b, \qquad (11)$$

$$\left(\Omega - i\frac{1}{\tau_2}\right)e_q + g_a e^{i\theta}e_a + g_b e^{-i\theta}e_b = \omega e_q. \qquad (12)$$

Integrating the above equations, the set equations are obtained as follows:

$$-iv_g(t_u - 1) + V_a e_a = 0, \qquad (13)$$

$$-iv_g r_u + V_b e_b = 0, \qquad (14)$$

$$\left(\omega_c - i\frac{1}{\tau_a}\right)e_a + \frac{V_a^*}{2}(1 + t_u) + g_a e^{-i\theta}e_q + re^{-i\xi}e_b = \omega e_a, \qquad (15)$$

$$\left(\omega_c - i\frac{1}{\tau_b}\right)e_b + \frac{V_b^*}{2}r_u + g_b e^{i\theta}e_q + re^{i\xi}e_a = \omega e_b, \qquad (16)$$

$$\left(\Omega - i\frac{1}{\tau_2}\right)e_q + g_a e^{i\theta}e_a + g_b e^{-i\theta}e_b = \omega e_q. \qquad (17)$$

Finally, the main parameters denoting the transmission and reflection properties (t_u and r_u) are calculated as

$$r_u = \frac{-i2\Gamma\left(\omega - \Omega + i\frac{1}{\tau_2}\right)\left[g_a g_b e^{i2\theta} + r e^{i\xi}\left(\omega - \Omega + i\frac{1}{\tau_2}\right)\right]}{\alpha_a \alpha_b - g_a^2 g_b^2 - r^2\left(\omega - \Omega + i\frac{1}{\tau_2}\right)^2 - g_a g_b r \cos(2\theta - \xi)\left(\omega - \Omega + i\frac{1}{\tau_2}\right)}, \tag{18}$$

$$t_u = \frac{\alpha_b\left[\left(\omega - \Omega + i\frac{1}{\tau_2}\right)\left(\omega - \omega_a - g_a^2\right)\right] - g_a^2 g_b^2 - r^2\left(\omega - \Omega + i\frac{1}{\tau_2}\right)^2 - g_a g_b r \cos(2\theta - \xi)\left(\omega - \Omega + i\frac{1}{\tau_2}\right)}{\alpha_a \alpha_b - g_a^2 g_b^2 - r^2\left(\omega - \Omega + i\frac{1}{\tau_2}\right)^2 - g_a g_b r \cos(2\theta - \xi)\left(\omega - \Omega + i\frac{1}{\tau_2}\right)}, \tag{19}$$

with $|V_a| = |V_b| = V$, $\Gamma = V^2/(2V_g)$, $\alpha_a = (\omega - \Omega + i\frac{1}{\tau_2})(\omega - \omega_a + i\frac{1}{\tau_a} + i\Gamma) - g_a^2$, and $\alpha_b = (\omega - \Omega + i\frac{1}{\tau_2})(\omega - \omega_b + i\frac{1}{\tau_b} + i\Gamma) - g_b^2$.

These analytical results of the amplitudes provide a complete description of the single-photon transport properties. Typically, without intrinsic loss, $T + R = 1$ is satisfied to obey the probability conservation of the single excitation. To realize UPSP under-non-ideal chiral photon-atom interactions, the reflection amplitude of r_u needs to be significantly suppressed, while the transmission amplitude remains high. As shown in Eq. (18), we can see that the reflection amplitudes include two paths, wherein photons in one path are emitted by the atom and are coupled to the mode b and photons in the other path are scattered from mode a to mode b by the scatterer. It can be seen from Eq. (18) that the amplitudes of the two paths have different phases and result in constructive or destructive interferences between them depending on the practical parameters. Given that the coupling strengths between the atom and the WGMM are fixed, both the frequency of the incident photon (i.e., ω) and the coupling strength between the scatterer and the WGMM can be precisely modulated. For example, the position of the scatterer can be controlled by a nanopositioner, and thus, $re^{i\xi}$ can be finely tuned to result in destructive interference between the mode b photons from two different paths [45–47]. Specifically, when $re^{i\xi} = -g_a g_b e^{i2\theta}/(\omega - \Omega + i\frac{1}{\tau_2})$, the mode b photons from two paths have the same amplitudes but have a phase difference of π. This results in perfect destructive interference, and then the UPSP is realized. In the following, the interference effect of the interplay between chirality and backscattering will be demonstrated in the rest of the work.

III. UNIDIRECTIONAL TRANSMISSION OF SINGLE PHOTONS UNDER NONIDEAL CHIRAL PHOTON-ATOM INTERACTIONS

First, we investigate the single photon scattered by the WGMM-atom-scatterer-waveguide system with nonideal chiral photon-atom iterations by ignoring the dissipations (i.e., $1/\tau_a = 1/\tau_b = 1/\tau_2 = 0$). Considering the photon-atom coupling is in the strong coupling regime with $g_a = 3\Gamma$, $g_b = 0.6\Gamma$, $\Omega = \omega_c$, and $\Delta = \omega - \omega_c = \omega - \Omega$.

Before we proceed, we briefly outline some of the main features of the transmission and reflection amplitudes of Eqs. (18) and (19). When the two-level atom is coupled to the WGMM with ideal chiral photon-atom interactions and without the scatterer, i.e., $g_b = 0$ and $r = 0$, resonant photons ($\Delta = 0$) are always perfectly transmitted with $T = 1$. Physically, all the emitted photons are coupled to mode a, which

results from the destructive interference between the emitted photon and the directed transmitted photon with $T = 1$ [50]. Specifically, when the scatterer is coupled to the WGMM (i.e., $g_b = 0$ and $r > 0$), the incident photon is also transmitted. It can be deduced from Eq. (19) that when $\Delta = 0$ and $g_b = 0$, $T = 1$ regardless of the coupling between mode a and mode b. Although the mode b photon of the left circular polarization is created by the scatterer, the mode b photon does not interact with the atom of the σ_+ transition because the polarization of mode b is orthogonal to the atomic σ_+ transition. Therefore, UPSP is robust against scattering under ideal chiral photon-atom interactions. However, the properties are different when the coupling between the atom and the WGMM is nonideal chiral, as $g_a = 3\Gamma$, $g_b = 0.6\Gamma$, and $r = 0$. Because the atom is coupled to both WGMM modes a and b, the amplitude of the photon emitted by the atom coupled to mode a is less than that of the ideal chiral photon-atom interaction. The destructive interference between them results in suppressing the amplitude of the output photon along the waveguide with $T < 1$. When the scatterer is coupled to the WGMM with $r > 0$, the interference between photons from different paths will disturb the transporting properties, which will be demonstrated in detail.

As plotted in Fig. 2(a), with $\Delta = -0.225\Gamma$ and $\theta = 0.5\pi$, the position of the scatterer determining two parameters of r and ξ modulates the reflection properties, wherein an area of no reflection corresponding to small values of r is found. The details are shown in Fig. 2(b), with $\theta = 0.5\pi$ and $\xi = 1.0\pi$. As the backscattering strengths are increased, the amplitudes of the mode b photon produced by the scatterer are enhanced to strengthen the destructive interference so that the reflection probabilities are suppressed. When the value of the backscattering strength is increased to $r = 8.0\Gamma$, the perfect destructive interference required as $re^{i\xi} = -\frac{g_a g_b e^{i2\theta}}{\Delta}$ is satisfied. This directly results in $R = 0$. Further increasing the backscattering strength makes the amplitude of the photon from the scattering process larger than that from the atom, and then the perfect destructive interference is no longer satisfied with $R > 0$. In the limit of $r = 25\Gamma \gg g_a \gg \Gamma$, as shown in the inset of Fig. 2(b), the reflection probabilities in the WGMM-atom structure are the same as those in the empty WGMM with strong backscattering strengths, wherein R_e is the reflection spectra of the empty WGMM with $g_a = g_b = 0$. Physically, the modes of the WGMM split by the strong backscattering strengths lead to the atom decoupling to the WGMM, so the incident photon is totally transmitted with $R \approx 0$, which indicates that the incident photon does not interact with the WGMM-atom structure. Consequently, the transmission process can be divided into the interference regime ($r < 25\Gamma$) and the backscattering regime
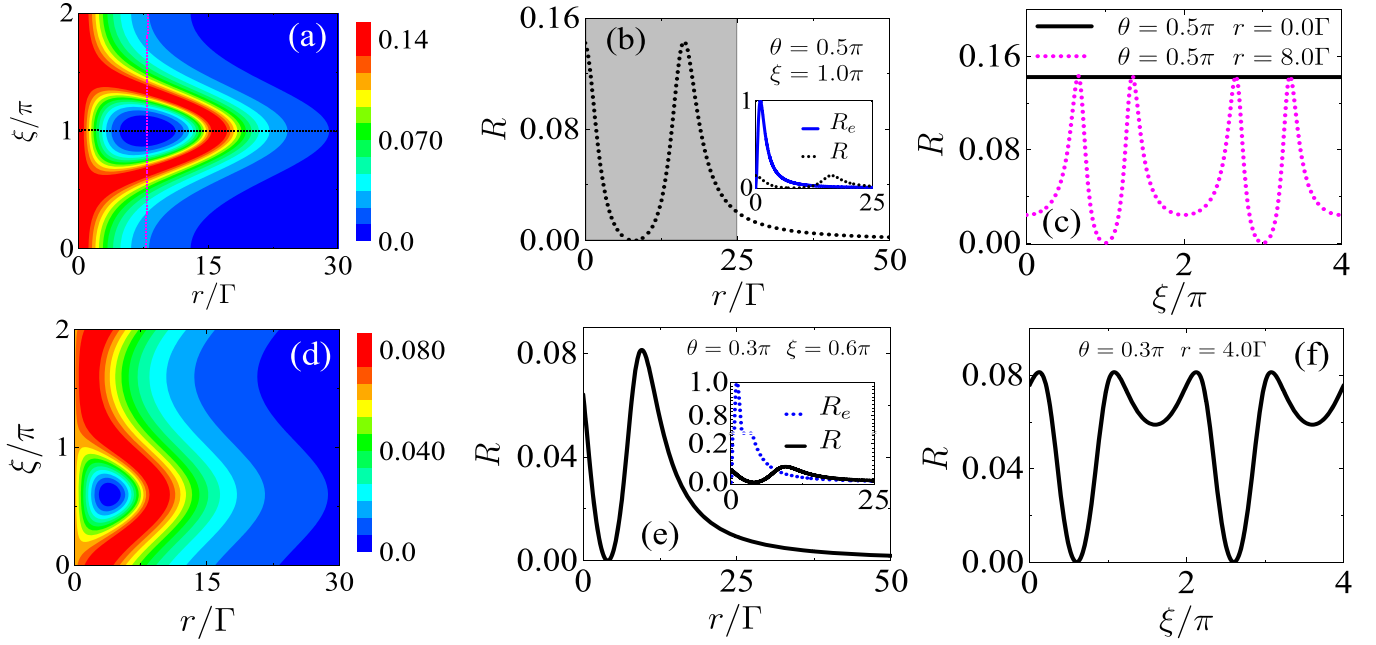
FIG. 2. Reflection spectra of the incident single photon under the nonideal chiral photon-atom interaction. $g_a = 3\Gamma$, $g_b = 0.6\Gamma$, $\theta = 0.5\pi$, and $\Delta = -0.225\Gamma$ in the upper part; $g_a = 3\Gamma$, $g_b = 0.4\Gamma$, $\theta = 0.3\pi$, and $\Delta = -0.3\Gamma$ in the lower part. The horizontal and vertical lines in (a) correspond to (b) and (c), respectively. R_e in the inset of (b) and (e) are the reflection spectra of the empty WGMM with $g_a = g_b = 0$ and then the reflection probabilities only depend on the coupling strength r between modes a and b. The results show that the interference between mode b photons from two paths can be used to realize the UPSP under the nonideal chiral photon-atom interaction by changing the position of the scatterer.

($r > 25\Gamma$). When perfect destructive interference occurs with $r = 8.0\Gamma$, the atom is actually coupled to the WGMM, and thus, the information of the atom carried by the single photon without backflow is exactly the kind of mechanism we need. Figure 2(c) demonstrates that, when the atom is coupled to the WGMM with nonideal chiral interactions and without introducing the scatterer of $r = 0$, the reflection of the incident photon is unavoidable as $R > 0$. In contrast, when $r = 8.0\Gamma$, the UPSP can also be obtained by changing the position of the scatterer along the WGMM to vary the relative distance between the scatterer and the atom.

The above conclusions are regardless of the parameters, such as the coupling strengths between the atom and the WGMM (i.e., g_a, g_b, and θ). For example, as shown in Fig. 2(d), when the system is fixed with $g_a = 3.0\Gamma$, $g_b = 0.4\Gamma$, and $\theta = 0.3\pi$, the total transmission area is also found at the frequency detuning of $\Delta = -0.3\Gamma$. The corresponding perfect destructive interference occurs with a much smaller backscattering strength of $r = 4.1\Gamma$, as shown in Fig. 2(e). Specifically, the enhancement of reflection probabilities is found to be $R(r = 9.5\Gamma) > R(r = 0)$. This indicates that the amplitude of b photons scattered from the a photon is more than double that of the emitted photons, and thus, the interference between them leads to enhancement. The inset of Fig. 2(e) demonstrates that (i) when the backscattering strength is around the perfect destructive interference point, there are significant differences between R_e and R. This means that the interference is directly produced by the interplay between chirality and backscattering, wherein mode splitting is not dominant and both the atom and the scatterer are coupled to the WGMM. (ii) When the backscattering strengths

are much larger than the atom-WGMM coupling strengths (i.e., $r = 25\Gamma$), the system is changed into the backscattering regime and then both two kinds of reflections are suppressed to $R \approx R_e \approx 0$. The UPSP can also be realized by controlling the relative position of the scatterer with a small backscattering strength of $r = 4.0\Gamma$, as illustrated in Fig. 2(f). Therefore, even when the photon-atom interaction is nonideal chiral, UPSP is able to be realized by adjusting the position of the scatterer and changing of the frequency of incident photons.

Next, we investigate the UPSP influenced by the frequency detuning of the incident photons. As shown in Fig. 3(a), with $\theta = \xi = 0$, the reflection spectra can be controlled from 0 to 100% by properly tuning the positions of the scatterer and adjusting the frequency of the photon. Perfect destructive interferences demonstrated as $R = 0$ still arise with detuned frequencies. When $\theta = 0$ and $\xi = 0.5\pi$, the reflection spectra are symmetrical to the resonant frequency, as shown in Fig. 3(b). Specifically, the reflection properties of resonant photons are insensitive to the backscattering strengths. It can be deduced from Eqs. (18) and (19) that when $2\theta - \xi = (n + \frac{1}{2})\pi$, $n = \pm 1$, ± 2, ..., the transmission and reflection amplitudes of resonant photons with $\Delta = 0$ do not depend on the backscattering strength r. The behaviors are demonstrated in Fig. 3(c) in detail. With $g_b = 0.6\Gamma$ and $r = 0$, due to the atom coupled to both WGMM modes, the transmission spectra have three dips. Physically, the two counterpropagating modes of the WGMM are through linear superposition and can alternatively be described as two standing-wave modes. One of the standing-wave modes has a minimum amplitude at the position of the atom, and thus corresponds to the middle dip of $\Delta = 0$. The other standing-wave mode at the position
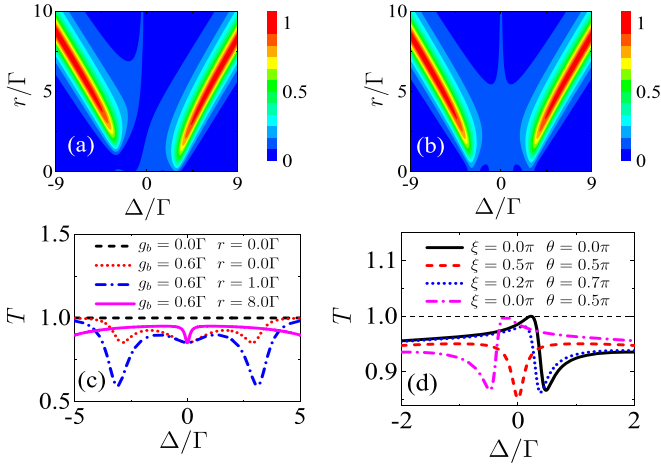
FIG. 3. Reflection spectra as Δ and r varied in (a) and (b). Transmission spectra for different r and phases in (c) and (d). $\theta = 0$ and $\xi = 0$ in (a); $\theta = 0$ and $\xi = 0.5\pi$ in (b); $\theta = \xi = 0.5\pi$ in (c); $r = 8.0\Gamma$ in (d). Other parameters are $g_a = 3.0\Gamma$ and $g_b = 0.6\Gamma$. The symmetry of the spectra around the resonant frequency depends on the WGMM-atom and WGMM-scatterer coupling strengths.

of the atom does not have a minimum amplitude and experiences Rabi-like splitting by interacting with the atom. As the intermode coupling strength is increased, the two side dips resulting from the Rabi-like splitting are broadened. However, the central dip is not affected by the increase in r. This means that, although the strong backscattering strengths larger than the WGMM-atom and WGMM-waveguide coupling strengths split the transmission spectra obviously, the central mode still couples to the atom with unchanged coupling strengths. The fixed coupling strengths lead to transmission properties under $\theta = \xi = 0.5\pi$ having no relation to the backscattering strengths of r.

Then, we further investigate transmission spectra around the resonance with different phases around $\Delta = 0$. As shown in Fig. 3(d), when $\theta = \xi = 0.5\pi$, the transmission probabilities are symmetric about $\Delta = 0$. However, other choices of phases make the spectra change asymmetrically as Fano resonance [59–61]. Here, the scatterer adopted to backscatter the WGMM modes is equivalent to a mirror to reflect the photon [62].

IV. UNIDIRECTIONAL PROPAGATION OF SINGLE PHOTONS AGAINST DISSIPATIONS

Finally, the effects of dissipations on the interplay between chirality and backscattering are numerically investigated. In general, the unavoidable intrinsic dissipative processes in the waveguide-WGMM-atom system always result in the leakage of photons into the nonwaveguide modes. These dissipations directly disturb the interference between mode b photons from two different paths and then affect the transmission properties [63]. As demonstrated in Fig. 4(a), when a two-level atom is coupled to the WGMM with dissipations, the regions of $R = 0$ can also be found around the resonance by adjusting the positions of the scatterer. Typically, Figs. 4(b) and 4(c) show that the transmission contrast, evaluated as $D = \frac{T-R}{T+R}$ [12,64], can also be reached as $D = 1$ by adjusting Δ or ξ, and thus the incident photon is unidirectionally propagated to the right side of the waveguide with $R = 0$. This UPSP also results from the perfect destructive interference between the mode b photons from two paths with $R = 0$. The underlying physical mechanism is that the amplitude of the photon is influenced by the scatterer from mode a to mode b, so that the preconditions required for perfect destructive interference are satisfied. The required backscattering strength can be evaluated from Eq. (18) as $re^{i\xi} = -\frac{g_a g_b e^{i2\theta}}{\omega - \Omega + i/\tau_2}$. Therefore, the UPSP promoted here is a robust mechanism to overcome the influence of dissipations.

V. DISCUSSIONS AND CONCLUSION

To realize the above scheme in real experiments, two requirements should be prepared in advance. One requirement is that the position and backscattering strength of the scatter could be precisely tuned. Practically, silica nanotips as Rayleigh scattering engineered by wet etching of a tapered fiber are widely used to couple with the two WGMM modes [41,42,44–47,65]. Moving the nanotip towards the WGMM increases the overlap of the tip with the mode volume and enhances the backscattering strength. The position of the tip can be controlled by a nanopositioning stage with a resolution of nanometers for each step [45]. The other requirement is that a single atom can be deterministically coupled to the WGMM
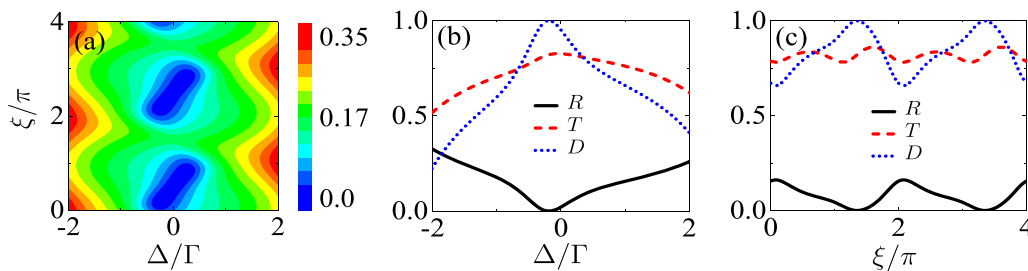

FIG. 4. Unidirectional propagation properties of single photons influenced by the dissipations. (a) Reflection spectra with dissipations. $1/\tau_a = 1/\tau_b = 1/\tau_2 = 0.2\Gamma$, $r = 3\Gamma$, $g_a = 2\Gamma$, $g_b = 0.4\Gamma$, and $\theta = 0$. Although the dissipations of the WGMM and the atom result in photons decaying into the environment, the regions of $R = 0$ can also be found around the resonance by adjusting the positions of the scatterer. (b) Unidirectional propagation contrast of single photons (defined as $D = \frac{T-R}{T+T}$) under the nonideal chiral photon-atom interaction against dissipations, with $\xi = 0.25\pi$. One perfect destructive interference is found at the reflection spectra, which guarantees the incident photon transporting to the right side of the waveguide without reflections. (c) Unidirectional propagation contrast of $D = 1$ can also be obtained by changing the relative positions of the scatterer, with $\theta = 0.3\pi$ and $\Delta = 0.2\Gamma$.

with nearly chiral photon-atom interactions. Recently, a deep-standing–wave-optical dipole trap created by retroreflecting a focused laser from the WGMM surface was demonstrated to trap a single Rb atom at a distance of 200 nm near the surface of the WGMM [34,66]. By applying a strong far-detuned laser (with σ_- circularly polarization) to a V-type Rb atom, the AC Stark effect results in the σ_- transition of the V-type Rb atom decoupling to WGMM [67,68]. Consequently, the WGMM can only couple to the σ_+ transition of the atom [28], as required in Fig. 1.

In conclusion, one scatterer coupled to the evanescent field of the WGMM is adopted to manipulate the single-photon transport along the waveguide-WGMM-atom system. When a two-level atom is coupled to the WGMM with nonideal chiral photon-atom interactions, the UPSP along the waveguide can be realized by changing the positions of the scatterer. Due to the amplitudes of the photon being affected by the scatterer, the above UPSP is preserved even including dissipations. Our proposal can be realized within the current photonic technologies, applicable to both neutral atoms and solid-state emitters. Based on the interplay between chirality and scatterer, the demonstrated UPSP mechanism may be applied to enhance the performance of unidirectional single-photon devices such as quantum memories, nonreciprocal photonic devices, and switches under nonideal chiral photon-atom interactions. Our work could also be extended to multiple atoms, as each atom could contribute to both chiral and scattering interactions, and the dynamics of the system are worth further investigation.

[1] P. Lodahl, S. Mahmoodian, and S. Stobbe, Interfacing single photons and single quantum dots with photonic nanostructures, Rev. Mod. Phys. **87**, 347 (2015).

[2] D. E. Chang, V. Vuletić, and M. D. Lukin, Quantum nonlinear optics-photon by photon, Nat. Photon. **8**, 685 (2014).

[3] X. Gu, A. F. Kockumb, A. Miranowicz, Y.-X. Liu, and F. Nori, Microwave photonics with superconducting quantum circuits, Phys. Rep. **718-719**, 1 (2017).

[4] D. Roy, C. M. Wilson, and O. Firstenberg, Colloquium: Strongly interacting photons in one-dimensional continuum, Rev. Mod. Phys. **89**, 021001 (2017).

[5] J. M. Arrazola, V. Bergholm, K. Brádler, T. R. Bromley, M. J. Collins, I. Dhand, A. Fumagalli, T. Gerrits, A. Goussev, L. G. Helt, J. Hundal, T. Isacsson, R. B. Israel, J. Izaac, S. Jahangiri, R. Janik, N. Killoran, S. P. Kumar, J. Lavoie, A. E. Lita *et al.*, Quantum circuits with many photons on a programmable nanophotonic chip, Nature (London) **591**, 54 (2021).

[6] H. J. Kimble, The quantum internet, Nature (London) **453**, 1023 (2008).

[7] S. Mahmoodian, P. Lodahl, and A. S. Sørensen, Quantum Networks with Chiral-Light–Matter Interaction in Waveguides, Phys. Rev. Lett. **117**, 240501 (2016).

[8] J. Borregaard, A. S. Sørensen, and P. Lodahl, Quantum networks with deterministic spin-photon interfaces, Adv. Quantum Technol. **2**, 1800091 (2019).

[9] J.-T. Shen and S. Fan, Coherent Single Photon Transport in a One-Dimensional Waveguide Coupled with Superconducting Quantum Bits, Phys. Rev. Lett. **95**, 213001 (2005).

[10] L. Zhou, Z. R. Gong, Y.-X. Liu, C. P. Sun, and F. Nori, Controllable Scattering of a Single Photon inside a One-Dimensional Resonator Waveguide, Phys. Rev. Lett. **101**, 100501 (2008).

[11] L. Zhou, L.-P. Yang, Y. Li, and C. P. Sun, Quantum Routing of Single Photons with a Cyclic Three-Level System, Phys. Rev. Lett. **111**, 103604 (2013).

[12] Y. Shen, M. Bradford, and J.-T. Shen, Single-Photon Diode by Exploiting the Photon Polarization in a Waveguide, Phys. Rev. Lett. **107**, 173902 (2011).

[13] H. Pichler, T. Ramos, A. J. Daley, and P. Zoller, Quantum optics of chiral spin networks, Phys. Rev. A **91**, 042116 (2015).

[14] I.-C. Hoi, C M. Wilson, G. Johansson, T. Palomaki, B. Peropadre, and P. Delsing, Demonstration of a Single-Photon Router in the Microwave Regime, Phys. Rev. Lett. **107**, 073601 (2011).

[15] K. Fang, Z. Yu, and S. Fan, Photonic Aharonov-Bohm Effect Based on Dynamic Modulation, Phys. Rev. Lett. **108**, 153901 (2012).

[16] L. Yuan, S. Xu, and S. Fan, Achieving nonreciprocal unidirectional single-photon quantum transport using the photonic Aharonov-Bohm effect, Opt. Lett. **40**, 5140 (2015).

[17] P. Lodahl, S. Mahmoodian, S. Stobbe, A. Rauschenbeutel, P. Schneeweiss, J. Volz, H. Pichler, and P. Zoller, Chiral quantum optics, Nature (London) **541**, 473 (2017).

[18] K. Y. Bliokh, F. J. Rodríguez-Fortuño, F. Nori, and A. V. Zayats, Spin-orbit interactions of light, Nat. Photon. **9**, 796 (2015).

[19] R. Mitsch, C. Sayrin, B. Albrecht, P. Schneeweiss, and A. Rauschenbeutel, Quantum state-controlled directional spontaneous emission of photons into a nanophotonic waveguide, Nat. Commun. **5**, 5713 (2014).

[20] J. Petersen, J. Volz, and A. Rauschenbeutel, Chiral nanophotonic waveguide interface based on spin-orbit interaction of light, Science **346**, 67 (2014).

[21] R. J. Coles, D. M. Price, J. E. Dixon, B. Royall, E. Clarke, P. Kok, M. S. Skolnick, A. M. Fox, and M. N. Makhonin, Chirality of nanophotonic waveguide with embedded quantum emitter for unidirectional spin transfer, Nat. Commun. **7**, 11183 (2016).

[22] I. Söllner, S. Mahmoodian, S. L. Hansen, L. Midolo, A. Javadi, G. Kiršanskė, T. Pregnolato, H. El-Ella, E. H. Lee, J. D. Song, S. Stobbe, and P. Lodahl, Deterministic photon-emitter

coupling in chiral photonic circuits, Nat. Nanotechnol. **10**, 775 (2015).

[23] P.-O. Guimond, H. Pichler, A. Rauschenbeutel, and P. Zoller, Chiral quantum optics with *V*-level atoms and coherent quantum feedback, Phys. Rev. A **94**, 033829 (2016).

[24] A. Grankin, P. O. Guimond, D. V. Vasilyev, B. Vermersch, and P. Zoller, Free-space photonic quantum link and chiral quantum optics, Phys. Rev. A **98**, 043825 (2018).

[25] C. Sayrin, C. Junge, R. Mitsch, B. Albrecht, D. O'Shea, P. Schneeweiss, J. Volz, and A. Rauschenbeutel, Nanophotonic Optical Isolator Controlled by the Internal State of Cold Atoms, Phys. Rev. X **5**, 041036 (2015).

[26] O. A. Iversen and T. Pohl, Strongly Correlated States of Light and Repulsive Photons in Chiral Chains of Three-Level Quantum Emitters, Phys. Rev. Lett. **126**, 083605 (2021).

[27] D. L. Hurst, D. M. Price, C. Bentham, M. N. Makhonin, B. Royall, E. Clarke, P. Kok, L. R. Wilson, M. S. Skolnick, and A. M. Fox, Nonreciprocal Transmission and Reflection of a Chirally Coupled Quantum Dot, Nano Lett. **18**, 5475 (2018).

[28] L. Tang, J. Tang, W. Zhang, G. Lu, H. Zhang, Y. Zhang, K. Xia, and M. Xiao, On-chip chiral single-photon interface: Isolation and unidirectional emission, Phys. Rev. A **99**, 043833 (2019).

[29] C. A. Downing, J. C. López Carreño, F. P. Laussy, E. del Valle, and A. I. Fernández-Domínguez, Quasichiral Interactions between Quantum Emitters at the Nanoscale, Phys. Rev. Lett. **122**, 057401 (2019).

[30] B. Lang, R. Oulton, and D. M. Beggs, Optimised photonic crystal waveguide for chiral light-matter interactions, J. Opt. **19**, 045001 (2017).

[31] B. Lang, D. P. S. McCutcheon, E. Harbord, A. B. Young, and R. Oulton, Perfect Chirality with Imperfect Polarization, Phys. Rev. Lett. **128**, 073602 (2022).

[32] S. Mahmoodian, K. Prindal-Nielsen, I. Söllner, S. Stobbe, and P. Lodahl, Engineering chiral light-matter interaction in photonic crystal waveguides with slow light, Opt. Mater. Express **7**, 43 (2017).

[33] C. Junge, D. O'Shea, J. Volz, and A. Rauschenbeutel, Strong Coupling between Single Atoms and Nontransversal Photons, Phys. Rev. Lett. **110**, 213604 (2013).

[34] X. Zhou, H. Tamura, T.-H. Chang, and C.-L. Hung, Coupling Single Atoms to a Nanophotonic Whispering-Gallery-Mode Resonator Via Optical Guiding, Phys. Rev. Lett. **130**, 103601 (2023).

[35] A. Liu, L. Xu, X.-B. Xu, G.-J. Chen, P. Zhang, G.-Y. Xiang, G.-C. Guo, Q. Wang, and C.-L. Zou, Proposal for low-power atom trapping on a gan-on-sapphire chip, Phys. Rev. A **106**, 033104 (2022).

[36] M. Scheucher, A. Hilico, E. Will, J. Volz, and A. Rauschenbeutel, Quantum optical circulator controlled by a single chirally coupled atom, Science **354**, 1577 (2016).

[37] I. Shomroni, S. Rosenblum, Y. Lovsky, O. Bechler, G. Guendelman, and B. Dayan, All-optical routing of single photons by a one-atom switch controlled by a single photon, Science **345**, 903 (2014).

[38] D. D. Sedov, V. K. Kozin, and I. V. Iorsh, Chiral Waveguide Optomechanics: First Order Quantum Phase Transitions with $\mathbb{Z}_3$ Symmetry Breaking, Phys. Rev. Lett. **125**, 263606 (2020).

[39] D. Martin-Cano, H. R. Haakh, and N. Rotenberg, Chiral Emission into Nanophotonic Resonators, ACS Photon. **6**, 961 (2019).

[40] S. Rosenblum, O. Bechler, I. Shomroni, Y. Lovsky, G. Guendelman, and B. Dayan, Extraction of a single photon from an optical pulse, Nat. Photon. **10**, 19 (2016).

[41] L. Chang, X. Jiang, S. Hua, C. Yang, J. Wen, L. Jiang, G. Li, G. Wang, and M. Xiao, Parity-time symmetry and variable optical isolation in active-passive-coupled microresonators, Nat. Photon. **8**, 524 (2014).

[42] B. Peng, Ş. K. Özdemir, M. Liertzer, W. Chen, J. Kramer, H. Yılmaz, J. Wiersig, S. Rotter, and L. Yang, Chiral modes and directional lasing at exceptional points, Proc. Natl. Acad. Sci. USA **113**, 6845 (2016).

[43] C.-L. Zou, Y. Yang, C.-H. Dong, Y.-F. Xiao, X.-W. Wu, Z.-F. Han, and G.-C. Guo, Taper-microsphere coupling with numerical calculation of coupled-mode theory, J. Opt. Soc. Am. B **25**, 1895 (2008).

[44] J. Zhu, Ş. K. Özdemir, L. He, and L. Yang, Controlled manipulation of mode splitting in an optical microcavity by two Rayleigh scatterers, Opt. Express **18**, 23535 (2010).

[45] W. Chen, Ş. K. Özdemir, G. Zhao, J. Wiersig, and L. Yang, Exceptional points enhance sensing in an optical microcavity, Nature (London) **548**, 192 (2017).

[46] C. Wang, X. Jiang, G. Zhao, M. Zhang, C. W. Hsu, B. Peng, A. D. Stone, L. Jiang, and L. Yang, Electromagnetically induced transparency at a chiral exceptional point, Nat. Phys. **16**, 334 (2020).

[47] A. O. Svela, J. M. Silver, L. D. Bino, S. Zhang, M. T. M. Woodley, M. R. Vanner, and P. Del'Haye, Coherent suppression of backscattering in optical microresonators, Light: Sci. Appl. **9**, 204 (2020).

[48] J.-T. Shen and S. Fan, Theory of single-photon transport in a single-mode waveguide. I. Coupling to a cavity containing a two-level atom, Phys. Rev. A **79**, 023837 (2009).

[49] J.-T. Shen and S. Fan, Theory of single-photon transport in a single-mode waveguide. II. Coupling to a whisperinggallery resonator containing a two-level atom, Phys. Rev. A **79**, 023838 (2009).

[50] S. Rosenblum, A. Borne, and B. Dayan, Analysis of deterministic swapping of photonic and atomic states through single-photon Raman interaction, Phys. Rev. A **95**, 033814 (2017).

[51] H. Zheng and H. U. Baranger, Persistent Quantum Beats and Long-Distance Entanglement from Waveguide-Mediated Interactions, Phys. Rev. Lett. **110**, 113601 (2013).

[52] C. Cohen-Tannoudji, B. Diu, and F. Laloë, *Quantum Mechanics* (Wiley, New York, 1977).

[53] L. Allen and J. H. Eberly, *Optical Resonance and Two-level Atoms* (Dover, New York, 1987).

[54] L. Mandel and E. Wolf, *Optical Coherence and Quantum Optics* (Cambridge University Press, Cambridge, England, 1995).

[55] K. Srinivasan, and O. Painter, Mode coupling and cavity-quantum-dot interactions in a fiber-coupled microdisk cavity, Phys. Rev. A **75**, 023814 (2007).

[56] S. Fan, Ş. E. Kocabaş, and J.-T. Shen, Input-output formalism for few-photon transport in one-dimensional nanophotonic waveguides coupled to a qubit, Phys. Rev. A **82**, 063821 (2010).

[57] M. Bradford, K. C. Obi, and J.-T. Shen, Efficient Single-Photon Frequency Conversion Using a Sagnac Interferometer, Phys. Rev. Lett. **108**, 103902 (2012).

[58] W. Z. Jia, Y. W. Wang, and Y.-X. Liu, Efficient single-photon frequency conversion in the microwave domain using superconducting quantum circuits, Phys. Rev. A **96**, 053832 (2017).

[59] U. Fano, Effects of Configuration Interaction on Intensities and Phase Shifts, Phys. Rev. **124**, 1866 (1961).

[60] M. F. Limonov, M. V. Rybin, A. N. Poddubny, and Y. S. Kivshar, Fano resonances in photonics, Nat. Photon. **11**, 543 (2017).

[61] B.-B. Li, Y.-F. Xiao, C.-L. Zou, Y.-C. Liu, X.-F. Jiang, Y.-L. Chen, Y. Li, and Q. Gong, Experimental observation of Fano resonance in a single whispering-gallery microresonator, Appl. Phys. Lett. **98**, 021116 (2011).

[62] S. Fan, Sharp asymmetric line shapes in side-coupled waveguide-cavity systems, Appl. Phys. Lett. **80**, 908 (2002).

[63] H. Zheng, D. J. Gauthier, and H. U. Baranger, Cavity-Free Photon Blockade Induced by Many-Body Bound States, Phys. Rev. Lett. **107**, 223601 (2011).

[64] K. Xia, G. Lu, G. Lin, Y. Cheng, Y. Niu, S. Gong, and J. Twamley, Reversible nonmagnetic single-photon isolation using unbalanced quantum coupling, Phys. Rev. A **90**, 043802 (2014).

[65] H. Lü, C. Wang, L. Yang, and H. Jing, Optomechanically Induced Transparency at Exceptional Points, Phys. Rev. Appl. **10**, 014006 (2018).

[66] E. Will, L. Masters, A. Rauschenbeutel, M. Scheucher, and J. Volz, Coupling a Single Trapped Atom to a Whispering-Gallery-Mode Microresonator, Phys. Rev. Lett. **126**, 233602 (2021).

[67] Y. Yang, M. Yang, K. Zhu, J. C. Johnson, J. J. Berry, J. V. D. Lagemaat, and M. C. Beard, Large polarization-dependent exciton optical Stark effect in lead iodide perovskites, Nat. Commun. **7**, 12613 (2016).

[68] T. A. Wilkinson, D. J. Cottrill, J. M. Cramlet, C. E. Maurer, C. J. Flood, A. S. Bracker, M. Yakes, D. Gammon, and E. B. Flagg, Spin-selective AC Stark shifts in a charged quantum dot, App. Phys. Lett. **114**, 133104 (2019).